Observation of a novel flow regime caused by finite electric wall conductance in an initially turbulent magnetohydrodynamic duct flow

Blishchik, Artem; Kenjereš, Saša

DOI
10.1103/PhysRevE.104.L013101

Publication date
2021

Document Version
Final published version

Published in
Physical Review E

Letter

Observation of a novel flow regime caused by finite electric wall conductance in an initially turbulent magnetohydrodynamic duct flow

Artem Blishchik and Saša Kenjereš*

Department of Chemical Engineering, Faculty of Applied Sciences, Delft University of Technology and J.M. Burgerscentrum Research School for Fluid Mechanics, Van der Maasweg 9, 2629 HZ Delft, The Netherlands

(Received 3 May 2021; accepted 28 June 2021; published 30 July 2021)

We present results of a series of numerical simulations of an initially fully developed turbulent flow of a liquid metal in a long duct under the influence of a constant uniform transverse magnetic field and various wall conductances (ranging from perfectly insulated to perfectly conducting walls). The changes in the wall conductance caused the appearance of novel flow regimes characterized by the coexistence of locally turbulent or laminar flow regions and a nonmonotonic behavior of the corresponding wall-friction coefficients. In contrast to the situation where an increase in the imposed magnetic field will lead to continuous suppression of turbulence and final complete relaminarization of the flow in a specific range of wall-conducting parameters, we also observe an apparent partial and complete turbulence regeneration from the magnetohydrodynamic-suppressed laminar state.

DOI: 10.1103/PhysRevE.104.L013101

Starting from the pioneering theoretical and experimental studies of Refs. [1,2], the magnetohydrodynamic (MHD) interactions (i.e., interactions between the flow of an electrically conducting fluid (liquid metal, electrolyte, or plasma) and an imposed magnetic field) play an important role in numerous physical phenomena in nature and technology (e.g., origin of planetary magnetic fields, continuous casting, crystal growth, liquid-metal blankets in fusion reactors, etc., [3]). Despite the progress of various experimental techniques in classical fluid mechanics in recent years, MHD-related experiments are still very challenging, especially if the local multiphysics information is needed (e.g., simultaneous measurements of the instantaneous velocity and its gradients, pressure, electric potential, and total current density). Experimental difficulties are caused by the nontransparency of liquid metals, limited spatial and temporal resolutions, as well as the inherently three-dimensional nature of interactions between the velocity and electromagnetic fields. Recent progress in the eddy-resolving numerical simulation techniques, such as direct numerical simulation (DNS) and large eddy simulation (LES) approach, have opened additional possibilities for analysis of complex MHD interactions [4,5]. The advanced numerical simulations of MHD phenomena can provide detailed insights into local reorganization of the flow, turbulence, corresponding electric potential and total current density, and their cross correlations. The latter are notoriously difficult to get from the current experimental approaches and of crucial importance for the development of the Reynolds-averaging based class of turbulence models suitable for practical industrial and technological applications [6–8]. In the great majority of cases presented in the literature, the central focus of the MHD numerical research aims to determine the transient and turbulent flow characteristics in generic configurations, such as pipe, duct, and channel flow, subjected to an external (uniform or partially imposed) magnetic field of different strengths and orientations where the walls are assumed to be perfectly electrically insulated or conducting [9–13]. However, in practical conditions, one has also to deal with the finite thickness and electrical conductivity of surrounding walls, which can significantly alter the electric current behavior in the entire configuration. This alternation of electric current will affect the distributions of the Lorentz force and, consequently, the velocity components. The inclusion of surrounding walls with a finite thickness and electric conductivity is associated with numerous difficulties in both experimental and numerical studies. For experiments, multiple modular setups are required to study the influence of walls with various parameters. For simulations, advanced numerical solvers need to be developed, which can include also solid wall regions (in addition to the flow domain) for calculations of the electric current and potential (so-called conjugate MHD phenomena). Although the distinct effects of finite wall thickness and electric wall conductivity on a laminar MHD flow were thoroughly investigated by Hunt [14], studies reporting on the effects of a wide range of aforementioned wall parameters on MHD turbulent flow are scarce in the literature. The impact of specific wall conductivity values in a combination with different magnetic field orientations on a laminar MHD duct flow was demonstrated in a numerical research of Ref. [15]. The formation of the M-shape velocity profile, typical to the duct flow with conductive walls, was observed. Effects of electrically conducting walls on rotating magnetoconvection were analyzed in numerical simulations of Ref. [16]. It was shown that initially oscillatory magnetoconvection can become steady when electrically conducting walls were imposed. The instabilities in an MHD duct flow with a constant wall conductivity were numerically and experimentally studied in Refs. [17,18], respectively. The onset of instabilities and jet detachments were found in good agreement between the experiments and the simulations. In experimental studies of Ref. [19], measurements of the single- and multiphase MHD flows in

*Corresponding author: S.Kenjeres@tudelft.nl

rectangular channels were performed. When one of the electrically insulated walls was replaced with a copper plate (finite conductance), a suppression of the turbulence intensity was observed. Numerical studies of the linear stability of fully developed MHD flow in a square duct with insulating Shercliff walls and thin electrically conducting Hartmann walls subjected to a uniform magnetic field were presented in Ref. [20]. The main conclusion was that the wall conductance ratio determined flow stabilization or destabilization—depending on the strength of the imposed magnetic field.

The main motivation of the present Letter is to fill an existing gap in the literature; we seek to provide a detailed insight into the effects of finite electric conductivity of surrounding walls on a turbulent MHD flow. We consider a single-phase flow of an incompressible electrically conductive fluid in an initially fully developed turbulent regime, subjected to the homogeneous transverse magnetic field. Because of the magnetic Reynolds number $\mathrm{Re_m} = u_0 D/\lambda \ll 1$ condition (where u_0 is the characteristic velocity, D is the characteristic length scale, and $\lambda = 1/\mu_0\sigma$ is the magnetic diffusivity), the one-way coupled MHD approach is used. The flow is described by conservation of mass, momentum, and Ohm's law for the moving media, respectively,

$$\nabla \cdot \mathbf{u} = 0, \tag{1}$$

$$\frac{\partial \mathbf{u}}{\partial t} + (\mathbf{u}\cdot\nabla)\mathbf{u} = -\frac{1}{\rho}\nabla p + \nu\nabla^2\mathbf{u} + \underbrace{\frac{1}{\rho}(\mathbf{j}\times\mathbf{B})}_{\mathbf{F^L}}, \tag{2}$$

$$\mathbf{j} = \sigma(-\nabla\phi + \mathbf{u}\times\mathbf{B}), \tag{3}$$

where $\mathbf{u}$ is the velocity, p is the pressure, $\mathbf{j}$ is the current density, ϕ is the electric potential, $\mathbf{B}$ is the imposed magnetic field, $\mathbf{F^L}$ is the Lorentz force, ν is the kinematic viscosity, ρ is the density, σ is the electrical conductivity. By imposing the $\nabla\cdot\mathbf{j} = 0$, the Ohm's law reduces to a simple Poisson equation for the electric potential as

$$\nabla^2\phi = \nabla\cdot(\mathbf{u}\times\mathbf{B}). \tag{4}$$

In contrast to the governing transport equations for mass and momentum, which are applied for the fluid domain, the electric potential equation needs to be extended as well to the surrounding walls of finite thickness (d) and conductivity (σ_S). Note that the interface condition needs to be satisfied, i.e., $\phi_L = \phi_S$ and $\sigma_L\partial\phi_L/\partial n = \sigma_S\partial\phi_S/\partial n$, where L and S indicate liquid (fluid) and solid (wall) domains, respectively, and n is the wall normal. The problem is fully defined by two characteristic nondimensional parameters: Reynolds ($\mathrm{Re} = u_0 D/\nu$) and Hartmann ($\mathrm{Ha} = BD\sqrt{\sigma/\rho\nu}$) numbers.

To be able to simultaneously solve the distribution of governing parameters (ϕ and $\mathbf{j}$) in both fluid and wall regions as well to conserve the current density, we have developed the integrated conjugate MHD solver by combining the four steps projection method, proposed in Ref. [21], and the grid-coupling approach to match the fluid and wall regions. A finite-volume in-house code based on the open-source OpenFOAM-extend is applied to solve the discretized form of the transport equations, Eqs. (1)–(4). The second-order central differencing scheme is applied for both diffusive and convective terms, whereas the time integration is performed by the second-order backward scheme. For additional numerical details, see Ref. [22].

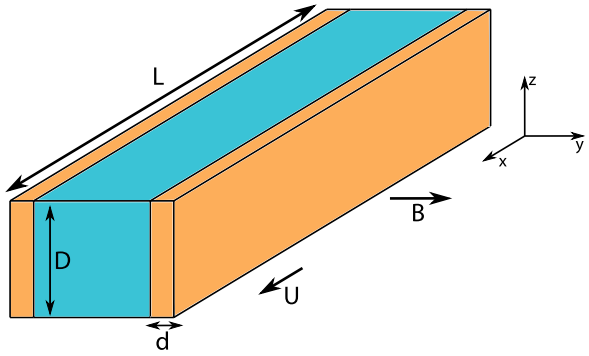

FIG. 1. Sketch of the simulation domain for the conjugate MHD duct flow.

All simulations are performed for the configuration shown in Fig. 1. We analyze the turbulent flow of an electrically conducting fluid (σ_L) in a long duct ($L = 40$ D) with a square cross-section ($D \times D$), surrounded by two walls with a finite thickness ($d/D = 0.05$), and an arbitrary electric conductivity (σ_S). The remaining upper and lower walls (Shercliff walls), parallel to the imposed magnetic field, are electrically insulated. At all walls, the no-slip velocity boundary condition is imposed. The flow is driven by the imposed pressure gradient in the streamwise x direction (periodic boundary condition), whereas the uniform magnetic field is imposed in the transverse y direction. The left- and right-surrounding walls (Hartmann walls), perpendicular to the imposed magnetic field, are characterized by a finite thickness and an arbitrary electric conductivity. These wall characteristics are incorporated into a single wall conductance ratio parameter, defined as $C_d = (\sigma_S d)/(\sigma_L D)$. In the present Letter, we covered an extensive range of the wall conductance parameter, i.e., $0 \leqslant C_d < \infty$, where $C_d = 0$ indicates fully electrically insulating walls, and $C_d \to \infty$ indicates the fully electrically conducting walls, respectively. For these two cases, boundary conditions for the electric potential are defined as: (i) $\partial\phi/\partial y = 0$ at $y = 0$ and $y = D$; $\partial\phi/\partial z = 0$ at $z = 0$ and $z = D$ for perfectly electrically insulated walls (all walls); (ii) $\phi = 0$ at $y = 0$ and $y = D$ for perfectly conducting (side) walls.

We apply the wall-resolving dynamic LES approach to capture the instantaneous turbulence structures. It serves as the best compromise between the accuracy in capturing the instantaneous flow physics and the total computational costs (in comparison to the fully resolving DNS [23,24]). The dynamic LES adopted here automatically takes into account the local effects of the Lorentz force generated, through local adjustment of the Smagorinsky coefficient [4,8]. The numerical mesh contains $(N_x \times N_y \times N_z = 720 \times 80 \times 80)_{\mathrm{fluid}}$ and $(N_x \times N_y \times N_z = 720 \times 12 \times 80)_{\mathrm{wall}}$ nonuniformly distributed control volumes in the fluid and wall regions, respectively. Special attention is devoted to having a proper resolution of boundary layers along the surrounding walls for all flow regimes. The Hartmann and Shercliff layer criteria (with a typical thickness of $\delta_{\mathrm{Ha}} = D/\mathrm{Ha}$ and $\delta_{\mathrm{Sh}} = D/\mathrm{Ha}^{1/2}$) have been accomplished with 10 points in the Hartmann layer and 25 points in the Shercliff layer.

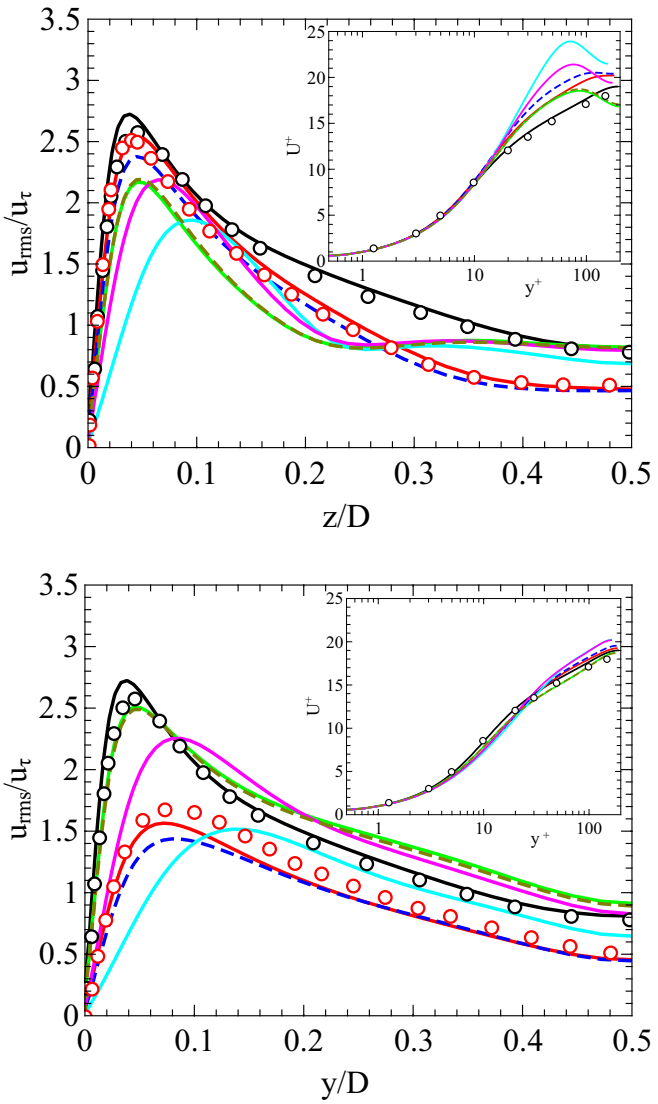

FIG. 2. Comparison of the present dynamic LES and DNS results from the literature for a non-MHD ((○): Ha = 0, [25]) and MHD ((○): Ha = 21.2, $C_d = 0$, [10]): (a) the vertical profiles in the proximity of the Shercliff walls, (b) the horizontal profiles in the proximity of the Hartmann walls of the nondimensional streamwise velocity fluctuations ($u_{\rm rms}$). The zoom ins show the logarithm-law distribution of the mean streamwise velocity component. The present dynamic LES is indicated as follows: (——): Ha = 0; (——): Ha = 21.2, $C_d = 0$; (– –) : Ha = 21.2, $C_d = 0.05$; (——): Ha = 21.2, $C_d = 0.25$; (——): Ha = 21.2, $C_d = 0.5$; (– –): Ha = 21.2, $C_d = 5$; (——): Ha = 21.2, $C_d \to \infty$.

We start our analysis by validating the dynamic LES approach adopted here against the fully resolved DNS results for a non-MHD duct flow (Ha = 0, [25]) and a MHD duct flow with perfectly electrically insulating walls ($C_d = 0$, Ha = 21.1, [10])— both in a fully developed turbulent regime at Re = 5602. The profiles obtained for the long-term time-averaged streamwise velocity fluctuations and the mean streamwise velocity component (characteristic logarithm-law distributions) are shown in Fig. 2. For both the non-MHD (Ha = 0) and the MHD case (Ha = 21.1), predicted profiles are in very good agreement with DNS results from the literature. Characteristic peak values in the proximity of walls are properly captured as well as the entire distribution towards the duct center—confirming the accuracy of the adopted simulation approach. Next, we move to perform a series of simulations by changing the wall-conductance ratio parameter (C_d) over an extensive range of values, varying from the electrically insulated to the perfectly electrically conducting walls, i.e., $0 \leqslant C_d < \infty$. All remaining flow parameters (Re and Ha) are kept unchanged. The first distinct feature of the profiles of the nondimensional streamwise fluctuating velocity is their peculiar nonmonotonic behavior, Fig. 2. The characteristic peak values in the proximity of the duct walls are observed for the non-MHD case with fully symmetric distributions along the Shercliff and Hartmann walls. Activation of the magnetic field with fully electrically insulated walls ($C_d = 0$) leads to small suppression of the peak value in the proximity of the Shercliff wall and a significant suppression in the proximity of the Hartmann wall. By slightly increasing the wall conductivity ($C_d = 0.05$), a small suppression of the peak values is observed in the proximity of both Hartmann and Shercliff walls, whereas the values in the duct center are unaffected. With $C_d = 0.25$, a suppression of the peak value is obtained in the proximity of the Shercliff walls. The location of the peak is shifted farther from the wall (i.e., at $z/L = 0.1$), and the value in the center of the duct is significantly increased, Fig. 2(a). In contrast to this behavior (for the same $C_d = 0.25$), the profile of streamwise velocity fluctuation in the vicinity of the Hartmann wall produced a peak value above that of $C_d = 0.05$, which is now shifted towards the duct center with higher values also in the central part of the duct, Fig. 2(b). For $C_d = 0.5$, a remarkable increase is observed at both locations. The value at the duct center reaches identical values as for the non-MHD case (i.e., Ha = 0). For $C_d = 5$, a less dramatic reorganization is taking place, characterized by the movement of the peak location closer to the walls, whereas the values in the duct center remain unaffected. With a further increase in $C_d \to \infty$, there are no visible additional changes in the profiles at both locations, indicating that a saturation point was reached.

To provide additional insights in this remarkable nonmonotonic behavior of the streamwise velocity fluctuations, we calculate the skin friction coefficients [$C_f = \tau/(0.5\rho u_0^2)$] at the Hartmann and Shercliff walls over a wide range of C_d, Fig. 3. Starting from a fully developed turbulent (T) state at Ha = 0, activation of the uniform transverse magnetic field at Ha = 21.2 with perfectly electrically insulating walls ($C_d = 0$), generates suppression of C_f at the Shercliff walls and an enhancement at the Hartmann walls. With a further increase in the wall conductivity, a gradual reduction in C_f is observed for both Hartmann and Shercliff walls (up to $C_d = 0.05$). After reaching $C_d = 0.05$, a more rapid suppression occurs for both walls, resulting in local minimum values in the $0.1 \leqslant C_d \leqslant 0.2$ range. The plots of the instantaneous streamwise velocity contours portray a stable fully symmetrical distribution without any traces of the locally occurring intermittency, indicating a complete relaminarization (L) of the flow, Fig. 3. After reaching $C_d > 0.2$, both friction coefficients start to increase. Analysis of the instantaneous streamwise velocity contours confirms the reappearance of the intermittent flow features. The slope of the C_f for the Shercliff walls is much steeper compared to the Hartmann walls, resulting in a characteristic crossover at approximately $C_d = 1$. For $C_d > 1$,

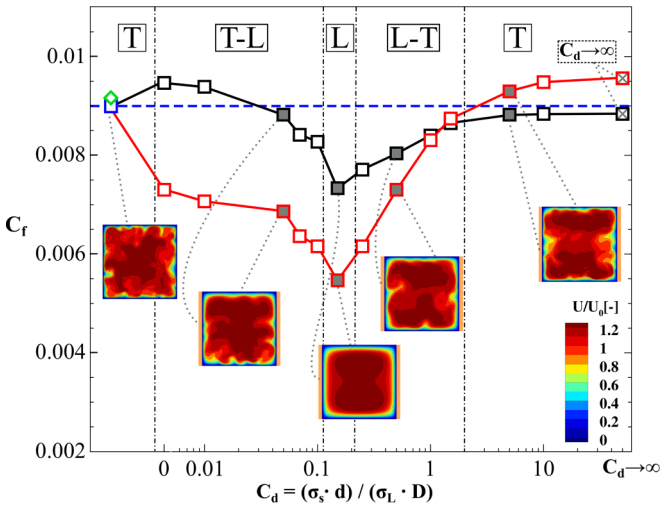

FIG. 3. Dependency of the friction coefficient (C_f) at the Shercliff (□) and Hartmann (□) duct walls on the wall-conductance parameter (C_d) for fixed Re = 5602 and Ha = 21.2. One representative of each characteristic flow regime is selected: (T): fully turbulent; (T-L): turbulent to laminar transition; (L): fully laminar; (L-T): laminar to turbulent transition, respectively. In the current plot, the value of C_f at the $C_d \to \infty$ regime has been assigned to a finite value of C_d instead of infinity. Furthermore, we indicate C_f values for the non-MHD case (Ha = 0): (□ — —): the present Letter; (◇): the experimental correlation of Ref. [26].

the friction coefficient at the Shercliff walls takes over its counterpart along the Hartmann walls, and a fully recovered turbulent state is present. Additional crossovers can be observed at $C_d = 5$ where the C_f along the Shercliff walls reaches the C_f of the non-MHD case. After $C_d = 5$, characteristic slopes are much less steep, indicating convergence towards the final asymptotic states. The values of C_f when $C_d \to \infty$, show an increase compared to the neutral non-MHD (Ha = 0) case for the Shercliff walls. In contrast to the Shercliff walls, C_f for the Hartmann walls reaches values close to the neutral case. It can be concluded that C_f behavior along the Hartmann and Shercliff walls portrays complex behavior indicating a significant flow and turbulence reorganization. Starting from the fully developed turbulent flow regime for the neutral non-MHD case by changing solely the wall conductance, the partial or complete relaminarization can be observed, followed by a rapid recovery of the intermittent states. Finally, for $C_d \to \infty$, the fully developed turbulence is recovered. Both of the previously analyzed quantities—the friction coefficients along the walls (Fig. 3) and profiles of the rms of the streamwise fluctuations (Fig. 2)—are long-term time-averaged quantities. We also partially addressed some of the instantaneous flow features by plotting contours of the streamwise velocity in the characteristic central plane (insets of Fig. 3). To provide detailed insights into a full three-dimensional flow and turbulence structures, we calculate the second invariant of the velocity-gradient tensor parameter (the so-called Q criterion), and apply this criterion to identify instantaneous features over a wide range of $0 \leqslant C_d < \infty$, Fig. 4. The plots reveal a very dense population of the coherent structures in the proximity of the Shercliff walls at the $C_d = 0$, Fig. 4(a). By changing the wall conductivity ($C_d = 0.05$ and $C_d = 0.1$) a distinct clustering of the coherent structures along the Shercliff walls is observed with a clear reduction of their spatial extent in the streamwise direction, Figs. 4(b) and 4(c). These distributions of the coherent structures exhibit similar patterns (patterned turbulence) as previously observed in standard MHD channels with electrically insulated walls ($C_d = 0$) when the strength of the imposed magnetic field is increased [12]. At $C_d = 0.15$, there is total suppression of the coherent structures, confirming full relaminarization of the flow, Fig. 4(d). For $C_d = 0.25$, reappearance of coherent structures in the central part of the duct takes place, confirming localized turbulence production, Fig. 4(e). By further increasing $C_d = 0.5$, the coherent structures start to occupy regions closer to the Shercliff walls, Fig. 4(f). This trend continues for higher values of $C_d = 1.5$ where coherent structures are rapidly expanding towards the wall regions (in both directions), producing even more dense distributions compared to the $C_d = 0$ case, Figs. 4(g) and 4(a). It should be noted that this is the range of C_d where C_f plots indicate a crossover between the Hartmann and the Shercliff walls, Fig. 3. There are no significant differences in coherent structure distributions between $C_d = 1.5$ [Fig. 4(g)] and the case with perfectly conducting walls, $C_d \to \infty$ [Fig. 4(h)].

To provide a possible origin of the observed changes of flow regimes—from initially fully turbulent, then partial and complete relaminarizations, and finally, return to fully recovered turbulence—we next analyze complex mechanisms

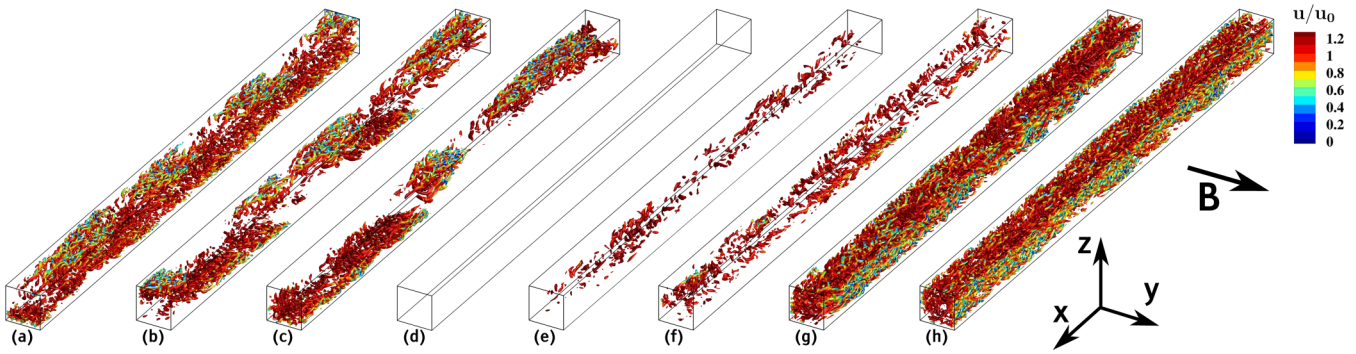

FIG. 4. The instantaneous coherent structures in the MHD duct flow identified as isosurfaces of the second invariant of the velocity-gradient tensor (Q criterion, $Q = 1\ \mathrm{s}^{-2}$), colored with the streamwise velocity at Re = 5602 and Ha = 21.2: (a) $C_d = 0$, (b) $C_d = 0.05$, (c) $C_d = 0.1$, (d) $C_d = 0.15$, (e) $C_d = 0.25$, (f) $C_d = 0.5$, (g) $C_d = 1.5$, and (h) $C_d \to \infty$.

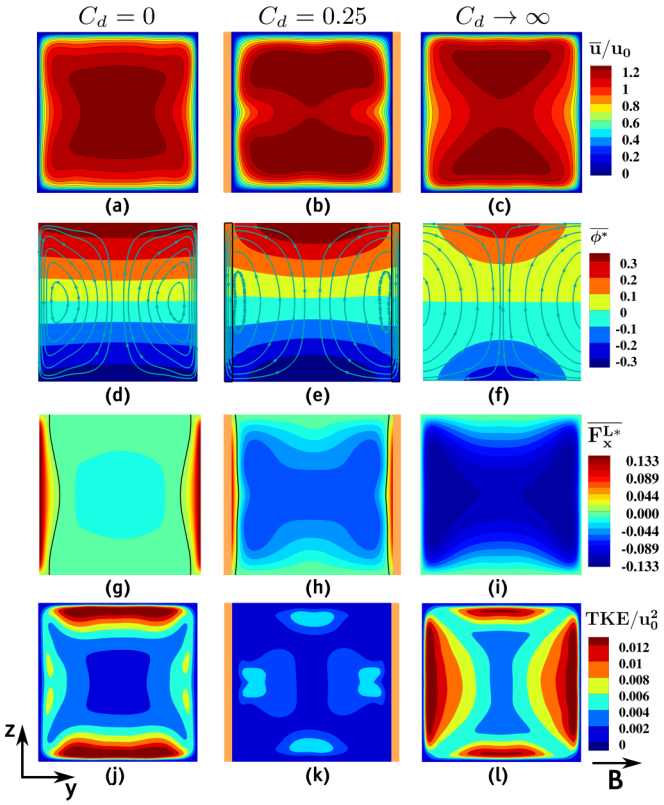

FIG. 5. Contours of the long-term time-averaged streamwise velocity (a)–(c), nondimensional electric potential ($\phi^* = \phi/U_0$BD) with iso-lines of electric current (d)–(f), the streamwise component of the nondimensional Lorentz force ($F_x^{L*} = F_x^L/\sigma U_0 B^2$) (g)–(i), and nondimensional turbulent kinetic energy (TKE $= 0.5\overline{u_i'^2}/U_0^2$) (j)–(l) in the central vertical plane ($x/L = 20$) for the fixed Re $= 5602$, Ha $= 21.2$, and various wall conductances.

along the following flow or electromagnetic field interaction pathways: $[\mathbf{u} \xrightarrow{\times \mathbf{B}} \nabla\phi \to \mathbf{e} \to \mathbf{j} \xrightarrow{\times \mathbf{B}} \mathbf{F^L} \to \mathbf{u}]$ (where $\mathbf{e}$ is the generated electric field). We plot contours of the mean streamwise velocity, electric potential, total current density, as well as resulting streamwise Lorentz force and turbulent kinetic energy—all on the central vertical plane ($L = 20$ D), Fig. 5.

For the fully insulated walls ($C_d = 0$), the mean streamwise velocity contours show a clear suppression along the central horizontal line, Fig. 5(a). The electric potential exhibits a nearly linear distribution in the vertical direction, Fig. 5(d). The total current streamlines form characteristic double loops which are closed within the fluid domain with the highest density in the proximity of the Hartmann walls, Fig. 5(d). These regions coincide with locations where the horizontal Lorentz force is highest, Fig. 5(g) due to mutual perpendicular orientation between the total current and the imposed magnetic field (note that the solid black line indicates the zero value of the F_x^{L*}) resulting in a significant reduction of turbulence here, Fig. 5(j). In contrast to this behavior, in the proximity of the Shercliff walls, the Lorentz force is much weaker, and the resulting turbulent kinetic energy is almost unaffected in comparison to the non-MHD case. The imprints of the generated Lorentz force on the mean streamwise velocity are shown in Fig. 5(a) where a transition from a full diagonal symmetrical distribution (for the non-MHD case) towards symmetry along the central vertical line is obtained. By replacing the fully insulated Hartmann walls with walls with the finite conductance ($C_d = 0.25$), different distributions of the mean velocity are obtained, showing two distinct regions aligned with the Shercliff walls, Fig. 5(b). Note that the selected value of $C_d = 0.25$ is for the case for which a local turbulence reoccurrence happens [as illustrated in Fig. 4(e)]. The total current streamlines are now entering the sidewalls, and the electric potential starts to increase gradients in the corner regions, Fig. 5(e). The resulting positive streamwise Lorentz force is confined within much thinner Hartmann boundary layers, whereas the significant negative Lorentz force is generated in the duct center, Fig. 5(h). The regions with the positive streamwise Lorentz force disappear entirely for $C_d \to \infty$, Fig. 5(i). The strong shear originating from the M-shaped velocity profiles re-introduces the turbulence seed regions farther away from the boundary layer regions, generating the four distinct islands of the elevated turbulence, Fig. 5(k). With a further increase in C_d, these regions expand toward walls, producing the final ($C_d \to \infty$) turbulence distribution as shown in Fig. 5(l). In contrast to $C_d = 0$ case (Fig. 5(j), the turbulence along the Hartmann walls is augmented—in both intensity and area that occupies. The turbulence along the Shercliff walls now covers a significantly smaller area, Fig. 5(l). Despite this locally enhanced turbulence region, the friction coefficient (C_f) along the Hartmann walls is smaller than along the Shercliff walls, Fig. 3. This confirms that the observed nonmonotonic changes in the friction coefficients along the Hartmann and Shercliff walls are the result of combined effects of the generation of the distinct wall-jet regions in the proximity of the Shercliff walls (i.e., M-shaped mean streamwise velocity profiles) and turbulence reorganization. Our argument that the combined effects are responsible for the observed novel regimes are also supported by the fact that a monotonic behavior of the friction coefficient versus wall-conductance dependency (i.e., continuously increasing for the Shercliff walls and continuously decreasing for the Hartmann walls) is obtained for the laminar MHD duct cases with changing wall conductance in the $0 \leqslant C_d < \infty$ range [22].

To summarize, we numerically investigated the influence of varying the electric conductance of surrounding duct walls on the initially fully developed turbulence subjected to a transverse constant uniform magnetic field. We analyzed the instantaneous and long-term time-averaged features of the flow, turbulence, electric potential, total current density, and resulting Lorentz force. The instantaneous coherent structures portray distinct regimes characterized by a coexistence of the turbulent and laminar flow regimes, a complete relaminarization, as well as a partial and complete turbulence regeneration. This nonmonotonic behavior was also reflected in the distributions of the friction coefficients along the Hartmann and Shercliff walls. The initially higher values of C_f along the Hartmann walls and lover values along the Shercliff walls for $C_d = 0$ are inverted for $C_d \to \infty$. The characteristic crossover occurred when $C_d \approx 1$. This behavior is explained in terms of combined reorganization of the main flow (wall jets) and local turbulence. The presented results can be directly applicable for the electromagnetic braking in continuous casting of

liquid steel and design of the liquid-metal blankets in a new generation of fusion reactors. Finally, with the present Letter, we would like to motivate a new generation of the MHD experiments in generic configurations based on here presented working conditions.

This project has received funding from the European Union's Horizon 2020 Research and Innovation Program TOMOCON (Smart tomographic sensors for advanced industrial process control) under the Marie Skłodowska-Curie Grant Agreement No. 764902.

[1] J. Hartmann, Kgl. Dan. Vidensk. Selsk. Mat. Fys. Medd. **15**, 1 (1937).
[2] J. Hartmann and F. Lazarus, Kgl. Dan. Vidensk. Selsk. Mat. Fys. Medd. **6**, 1 (1937).
[3] P. A. Davidson, *An Introduction to Magnetohydrodynamics* (Cambridge University Press, Cambridge, U.K., 2001).
[4] B. Knaepen and R. Moreau, Annu. Rev. Fluid Mech. **40**, 25 (2008).
[5] O. Zikanov, D. Krasnov, T. Boeck, A. Thess, and M. Rossi, Appl. Mech. Rev. **66**, 030802 (2014).
[6] A. Yoshizawa, *Hydrodynamic and Magnetohydrodynamic Turbulent Flows: Modelling and Statistical Theory* (Kluwer, Dordrecht, 1998).
[7] S. Kenjereš, K. Hanjalić, and D. Bal, Phys. Fluids **16**, 1229 (2004).
[8] S. Kenjereš, Int. J. Heat and Fluid Flow **73**, 270 (2018).
[9] D. Krasnov, O. Zikanov, J. Schumacher, and T. Boeck, Phys. Fluids **20**, 095105 (2008).
[10] R. Chaudhary, S. P. Vanka, and B. G. Thomas, Phys. Fluids **22**, 075102 (2010).
[11] D. Krasnov, O. Zikanov, and T. Boeck, J. Fluid Mech. **704**, 421 (2012).
[12] D. Krasnov, A. Thess, T. Boeck, Y. Zhao, and O. Zikanov, Phys. Rev. Lett. **110**, 084501 (2013).
[13] O. Zikanov, D. Krasnov, T. Boeck, and S. Sukoriansky, J. Fluid Mech. **867**, 661 (2019).
[14] J. C. R. Hunt, J. Fluid Mech. **4**, 557 (1965).
[15] A. Sterl, J. Fluid Mech. **216**, 161 (1990).
[16] K. Zhang and M. Weeks, Phys. Fluids **16**, 2023 (2004).
[17] T. Arlt and L. Bühler, Magnetohydrodynamics **55**, 319 (2019).
[18] L. Bühler, T. Arlt, T. Boeck, L. Braiden, V. Chowdhury, D. Krasnov, C. Mistrangelo, S. Molokov, and J. Priede, IOP Conf. Ser.: Mater. Sci. Eng. **228**, 012003 (2017).
[19] S. Eckert, Ph.D. thesis, Technical University of Dresden, Germany, 1998.
[20] T. Arlt, J. Priede, and L. Bühler, J. Fluid Mech. **822**, 880 (2017).
[21] M-J. Ni, R. Munipalli, P. Huang, N. B. Morley, and M. A. Abdou, J. Comp. Phys. **227**, 205 (2007).
[22] A. Blishchik, M. van der Lans, and S. Kenjereš, Int. J. Heat Fluid Flow **90**, 108800 (2021).
[23] D. K. Lilly, Phys. Fluids **4**, 633 (1992).
[24] S. B. Pope, New J. Phys. **6**, 35 (2004).
[25] S. Gavrilakis, J. Fluid Mech. **244**, 101 (1992).
[26] O. C. Jones, J. Fluids Eng. **98**, 173 (1976).